ACS OMEGA

http://pubs.acs.org/journal/acsodf

Article

Easily Constructed Imine-Bonded COFs for Iodine Capture at Ambient Temperature

Yonghe Sun, Sanan Song, Dehai Xiao, Linfeng Gan,* and Yuanrui Wang*

Cite This: *ACS Omega* 2020, 5, 24262−24271

Read Online

ACCESS | Metrics & More | Article Recommendations | Supporting Information

ABSTRACT: Volatile radionuclides generated during the nuclear fission process, such as iodine, pose risks to public safety and cause the threat of environmental pollution. Covalent organic framework (COF) materials have a controlled pore structure and a large specific surface area and thus demonstrate great opportunities in the field of radioactive iodine adsorption. However, the harsh synthetic conditions and the weak binding capability toward iodine have significantly restricted the applications of COFs in iodine adsorption. Here, we demonstrate a facile way to prepare a series of stable C−N-linked COFs with high efficiency to capture radioactive iodine species. Large-scale synthesis can be conducted by the aldol condensation reaction at room temperature. The resulting COFs have a large surface area and a strong resistance to acid, base, and water. Moreover, all types of COFs show high iodine adsorption, up to 2.6 g/g (260% in mass), owing to the large surface area and the functional groups in COFs. They not only absorb conventional I_2 molecular but also ionic state (I_3^- and I^+) iodine species. Theoretical calculations are further performed to understand the relationship between different iodine species and the functional groups of all COFs, offering the mechanisms underlying the potent adsorption abilities of COFs.

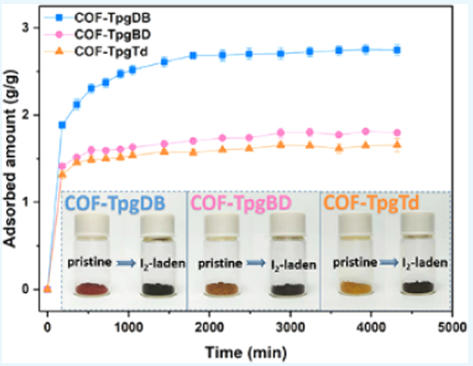

1. INTRODUCTION

Nuclear energy has many advantages over other sources of energy,[1,2] such as higher energy density and no emission of greenhouse gases. With plans of increasing the use of nuclear energy in many countries, safety concerns are coming to the fore. Especially, disposal of nuclear waste products and the rapid collection of nuclear leakage products in some extreme circumstances like in Fukushima plant have long been a challenge. The nuclear fission generates volatile radionuclides such as ^{3}H, ^{85}Kr, ^{129}I, and ^{131}I. Among them, radiological iodine has attracted particular attention because it has a long radioactive half-life (1.57×10^7 years for ^{129}I and 8.02 days for ^{131}I, respectively), high mobility, and adverse effects on the human metabolic system.[3] Developing a highly effective method for the capture and storage of radioiodine is urgently needed.

The physicochemical interactions between radiological iodine and adsorbent materials are critical to the adsorbent's capturing ability. It is necessary to point out here that neutral iodine molecule (I_2) can be readily converted into ionic state molecules,[4−7] following $(n + 1)I_2 \rightarrow I^-{\cdot}nI_2 + I^+$. A good radiological iodine adsorbent must have a good capability to capture both neutral iodine molecules and ionic state molecules. Currently, the prevalent methods to capture and store radiological iodine involve the use of reactive silver (Ag) adsorbent,[8,9] such as sliver-exchanged zeolites[10] and silver-functionalized silica aerogels.[11,12] These adsorbent materials can convert radiological iodine into strong interaction ionic compound AgI, but the use of silver in these materials raises further concerns about cost and environmental impact. Meanwhile, several adsorbent materials that have a higher affinity, higher loading capacity, and lower cost have been reported, such as metal−organic frameworks (MOFs),[13−16] melamine−formaldehyde polymers (MFPs),[17] and porous organic polymers (POPs).[18−26] For instance, James and his co-workers found that zeolitic imidazolate framework-8 (ZIF-8) showed excellent chemisorption to neutral iodine. Wang et al.[17] reported a high I_3^- ionic unit-loaded MFPs with controlled available surface areas, special structures, and designable functional groups. Inspired by Wang and her co-workers, a material that has a controlled available surface area and manipulating functional groups should have an ideological iodine loading. Covalent organic frameworks (COFs), as a new type of POPs, have attracted increasing attention[27−34] due to their regular pore structures, high stability, large available surface areas, and facile designability. By carefully selecting high interaction constructor units for iodine, COFs can be

Received: May 21, 2020
Accepted: August 13, 2020
Published: September 16, 2020

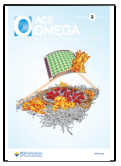

https://dx.doi.org/10.1021/acsomega.0c02382
ACS Omega 2020, 5, 24262−24271

used for capturing both neutral iodine molecular and ionic iodine molecular.[23,33,35,36] In the recent years, many COFs have been designed and synthesized for this purpose; for example, three-dimensional (3D) COF[34] consists of a diamond topology and heteropore/building unit COFs[21,35] with hollow microspheres. However, most of the COFs required rigorous synthesis conditions, such as synthesis in a flame-sealed ampoule and high temperature. The harsh synthetic conditions and the weak binding capability toward iodine have significantly restricted the large-scale applications of COFs in iodine adsorption.

Herein, we demonstrated a series of ultrastable C−N-linked COFs (CCOFs)[37−39] (COF-TpgDB, COF-TpgBD, and COF-TpgTd) with strong binding capabilities to I_2, I^+, I_3^-, and I_3^- and present in-depth investigations of the mechanism. In this study, all three CCOFs showed high chemical and thermal stabilities, as well as strong resistance toward acid, base, and water. As expected, the high-symmetry framework and large specific surface area of CCOFs permit iodine to diffuse through, fulfill, and trap in all of the cavities. Furthermore, density functional theory (DFT) calculations showed that the benzene ring, C═O, and −C−(NH)−C− unit in the COFs strongly interact with iodine species. Moreover, we propose a straightforward synthesis method of the C−N-linked CCOFs at room temperature that can facilitate the large-scale production for practical use without rigorous synthesis conditions.

2. RESULTS AND DISCUSSION

2.1. Experimental Results. *2.1.1. Chemical Structure and Compositions.* In this work, we have synthesized three C−N-rich COFs containing large amounts of amino groups to effectively construct porous materials with high iodine adsorption rates. The C−N linked COFs (Figure 1), COF-TpgDB, COF-TpgBD, and COF-TpgTd, have two different structures according to the previous study,[37,39] the enol form and the keto form, in a combination of reversible and irreversible organic reactions. Fourier transform infrared (FT-IR) analysis was carried out to confirm the amine formation. As shown in Figure 1a, compared to those of the starting materials, the peaks of amino N−H stretching bands (3100−3400 cm^{-1}) and aldehyde C═O stretching vibration (1685.5 cm^{-1}) of COF-TpgDB, COF-TpgBD, and COF-TpgTd disappeared completely, indicating that the starting materials were almost consumed or removed. The peaks at 1582.2 and 1282.9 cm^{-1} in the spectrum of COF-TpgDB are ascribed to the C═C stretching band and the C−N stretching vibration, respectively, indicating the presence of the keto form (Figure 1a). Meanwhile, no −OH and C═N characteristic stretching band appeared in the spectrum of COF-TpgDB, suggesting the complete transformation of the enol form into the keto form. Similarly, the peaks at 1596.2 cm^{-1} for COF-TpgBD and at 1598.4 cm^{-1} for COF-TpgTd corresponded to the C═C stretching band and that at 1284.7 cm^{-1} for COF-TpgBD and at 1282.2 cm^{-1} for COF-TpgTd was derived from the C−N stretching vibration. The −OH and C═N characteristic peaks also disappeared in the spectra of COF-TpgBD and COF-TpgTd, indicating that the keto forms are the dominant structures in COF-TpgBD and COF-TpgTd.

The structures of COF-TpgDB, COF-TpgBD, and COF-TpgTd were further confirmed by ^{13}C solid-state NMR spectroscopy. As shown in Figure 1b−d, these three CCOFs showed a distinct peak at about 180 ppm (184.3 ppm for

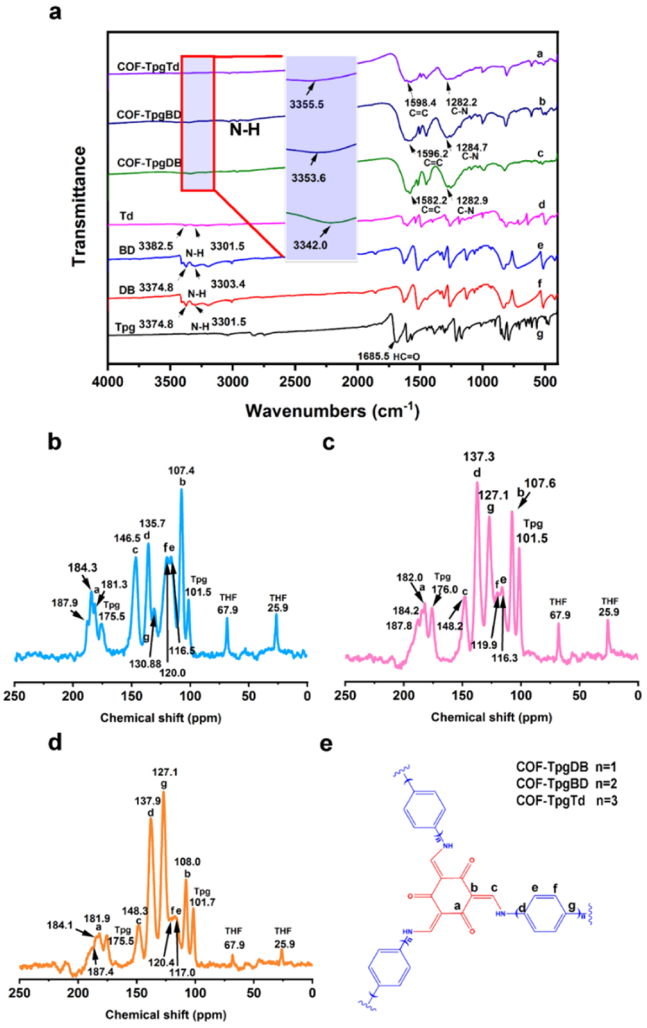

Figure 1. FT-IR and ^{13}C NMR spectra of CCOFs and starting materials. (a) IR spectra of Tpg, DB, BD, Td, COF-TpgDB, COF-TpgBD, and COF-TpgTd (from bottom to top). (b) ^{13}C NMR spectra of COF-TpgDB (blue). (c) ^{13}C NMR spectra of COF-TpgBD (red). (d) ^{13}C NMR spectra of COF-TpgTd (yellow). (e) Schematics of CCOFs.

COF-TpgDB, 181.8 ppm for COF-TpgBD, and 182.1 ppm for COF-TpgTd), corresponding to the carbon atoms in the carbonyl function groups. The signals at 181, 175, and 101 ppm were assigned to the carbon atoms of the starting material Tpg. The signals 67.9 and 25.1 ppm arise from the solvent tetrahydrofuran (THF) embedded in the CCOFs. Considering that all of the CCOF samples have been well purified and dried at 80 °C in vacuum for 72 h, small amounts of residual Tpg and THF might be trapped inside the deep cores of the CCOFs but cause no significant influence on the further experiments. Powder X-ray diffraction (PXRD) (Figure S1, see the Supporting Information) measurements with Cu Kα radiation were performed to verify the crystal structures of CCOFs. As illustrated in Figure S1, the presence of the obvious sharp diffraction peaks of each CCOF indicated that all these CCOFs were highly crystalline. A comparison of the experimental results with theoretical simulations showed that all CCOFs tended to have an eclipsed layered-sheet arrangement, which was consistent with the findings of previous studies.[37,39] This eclipsed layered-sheet CCOFs have more available surface area than the staggered ones, which would

https://dx.doi.org/10.1021/acsomega.0c02382
ACS Omega 2020, 5, 24262−24271

promote the iodine species to pass through and increase the adsorption efficiency.

Based on the above results, as the size of the triangular building unit increases from COF-TpgDB to COF-TpgTd, the pore size becomes larger. Here, we defined the pore size as the distance between two opposite edges in the hexagonal pore cross section. The pore dimension of COF-TpgDB, COF-TpgBD, and COF-TpgTd were 18.4 × 20.6, 26.0 × 29.0, and 33.0 × 37.9 Å^2, respectively. Nitrogen adsorption−desorption test at 77 K was carried out to characterize the porosity and porous structure of CCOFs. All COF samples showed a typical II adsorption isotherm (Figure S2). At a lower relative pressure of P/P_0 < 0.05, the adsorption amount increased sharply, showing a convex curve. The CCOF pore property parameter values are shown in Table S1. As shown in Figure S2d−f, the same N_2 adsorption isotherms illustrated that the Brunauer−Emmett−Teller (BET) surface areas of COFs were 209.6, 217.9, and 303.6 m^2 g^{-1} corresponding to COF-TpgDB, COF-TpgBD, and COF-TpgTd, respectively. These values are larger than those of some of the porous material molecular sieves. The pore size distributions of CCOFs were calculated based on the quenched solid density functional theory (QSDFT). The pore size was mainly distributed at 6.8, 8.3, and 9.9 nm for COF-TpgDB, COF-TpgBD, and COF-TpgTd, respectively. The pore volumes are about 0.36, 0.46, and 0.75 cm^3 g^{-1} for COF-TpgDB, COF-TpgBD, and COF-TpgTd, respectively. This result combined with the mainly distributed pore size of CCOFs, which are significantly larger than the theoretical ones and the transmission electron microscopy (TEM)/scanning electron microscopy (SEM) analyses, suggested that the inner cavities of CCOFs could be hollow microspheres.[35]

2.1.2. Stability of CCOFs. The thermogravimetric analysis (TGA) curve of COF materials is summarized in Figure S3. There was a small mass loss of the material after heating to 100 °C, which was mainly attributed to the evaporation of water and residuals solvent on the surface of CCOF materials and in the pore. At low temperature, the loss of mass results confirmed the FT-IR and ^{13}C NMR conclusions that the residual impurities were trapped deep in the CCOF cores. When the temperature was increased to 350 °C, the total weight loss rate of CCOFs was less than 12%. Even at 1000 °C, the weight loss rate of the material still remains below 57%. These results clearly suggested the good thermal stability of the as-prepared CCOF materials.

2.1.3. Iodine Adsorption Results. Iodine uptake of CCOFs was measured gravimetrically at various time intervals with triple parallel experiments. The iodine adsorption plot as a function of time is illustrated in Figure 2a. All three CCOFs showed a high iodine adsorption ability and a high adsorption ratio. The maximum adsorption capacities of iodine reached 2.75, 1.81, and 1.66 g/g for COF-TpgDB, COF-TpgBD, and COF-TpgTd, respectively. After the adsorption was completed, the color of the CCOFs changed from yellow or light yellow to black (Figure 2a inset). The iodine adsorption capacity of CCOFs was much higher than those of some of the traditional adsorption materials such as activated carbon and zeolite, making them attractive candidates in the field of iodine containment. It also needs to be pointed out that the adsorption rate of iodine was extremely fast during the period of 0−540 min, especially within the first 60 min, in which nearly 80% iodine was absorbed. The fast adsorption of CCOFs can be applied to emergency situations. To measure the iodine-containing ability of CCOFs, iodine-laden CCOFs

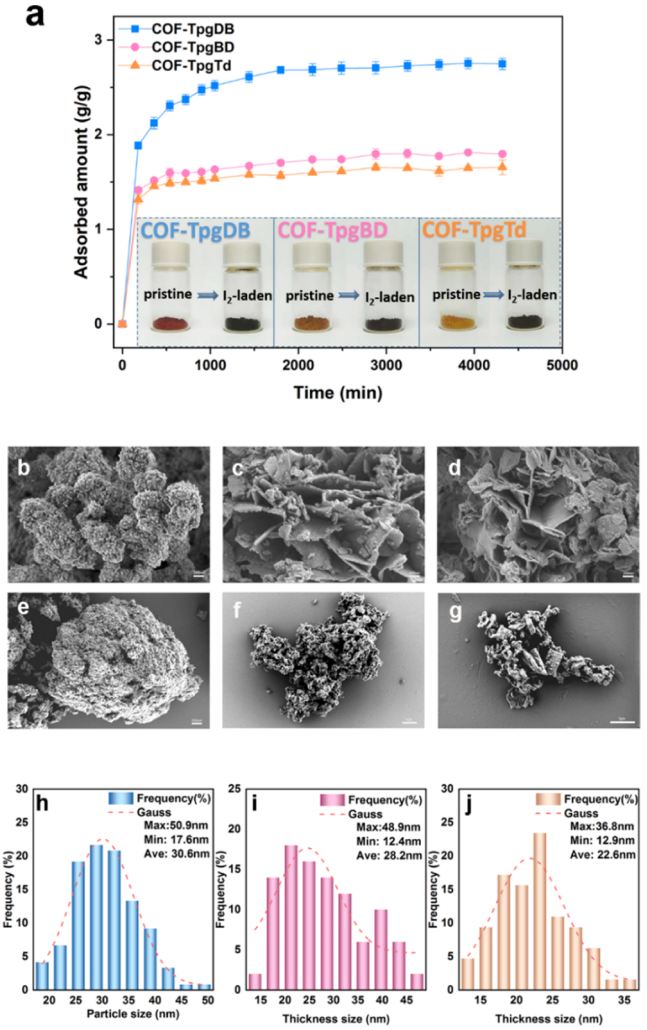

Figure 2. Analysis of iodine adsorption of CCOFs. (a) Adsorption isotherm of iodine versus contact time at 398 K, 1 bar; inset shows photographs before and after iodine adsorption. (b−d) SEM images of pristine COF-TpgDB, COF-TpgBD, and COF-TpgTd. (e−g) SEM images of I_2-laden COF-TpgDB, I_2-laden COF-TpgBD, I_2-laden COF-TpgTd. (h) Particle size distribution of COF-TpgDB, (i) thickness size distribution of COF-TpgBD, and (j) thickness size distribution of COF-TpgTd.

were sequentially washed with water and ethanol three times; at least 15% iodine remained in the CCOFs, revealing the long-term absorbing stability of CCOFs. The uptake of typical iodine adsorbents is summarized in Figure S4.

Scanning electron microscopy (SEM) images showed that COF-TpgDB (Figure 2b) exhibited a spherical morphology with a mean diameter of 30.6 nm (Figure 2h). COF-TpgBD and COF-TpgTd (Figure 2c,d) have lamellar structures with mean thicknesses of 28.2 and 22.6 nm (Figure 2I,j), respectively. After iodine adsorption, all CCOFs had different degrees of disruption collapse. Most COF-TpgDB (Figure 2e) agglomerate and some of the spheres were blasted, and the sheets of COF-TpgBD (Figure 2f) shrank into a cluster. However, COF-TpgTd (Figure 2g) retained the lamellar structure. To further understand the structural properties of CCOFs and iodine-laden CCOFs, transmission electron microscopy (TEM) combined with elemental mapping measurements was also applied to capture the detailed information about the CCOFs layers (Figures S5−S7). For

https://dx.doi.org/10.1021/acsomega.0c02382
ACS Omega 2020, 5, 24262−24271

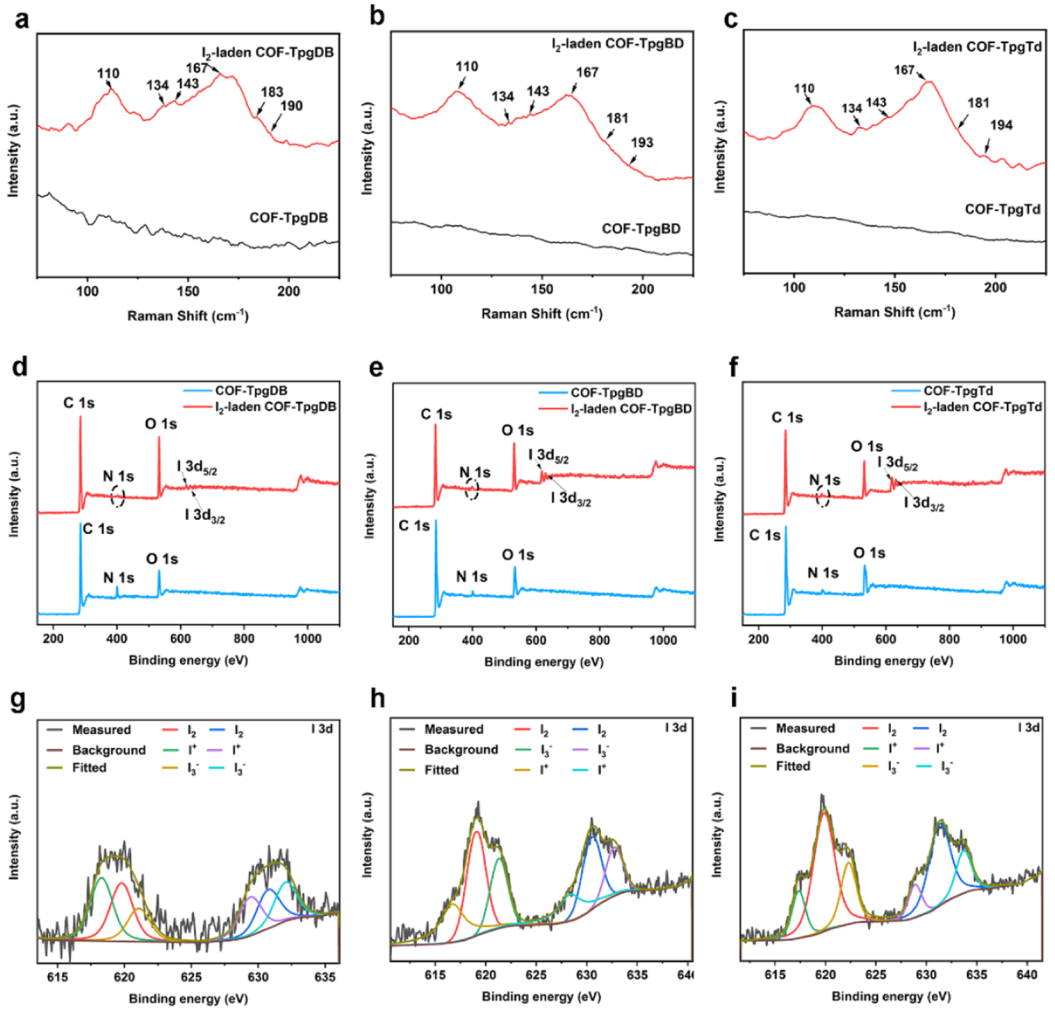

Figure 3. Raman and X-ray photoelectron spectra (XPS) of CCOFs and I_2-laden CCOFs. (a–c) Raman of I_2-laden CCOFs and CCOFs. (d–f) Survey XPS spectra of CCOFs and I_2-laden CCOFs. (g–i) Iodine high-resolution XPS spectra of I_2-laden COF-TpgDB, COF-TpgBD, and COF-TpgTd.

example, Figure S5a,b describes the pristine and iodine-laden COF-TpgDB structures. Figure S5c–h exhibits the high-angle annular dark field (HAADF)–scanning transmission electron microscopy (STEM) and elemental mapping images of the iodine-laden COF-TpgDB. Obviously, the iodine was filled with the COF-TpgDB pores. COF-TpgBD and COF-TpgTd also showed analogue iodine-loading properties (Figures S5–S7).

2.1.4. Absorbed Iodine Chemical State Analysis. Raman spectra were first recorded to reveal the iodine chemical state inside the pores of CCOFs (Figure 3a–c). Multiple peaks appeared in the iodine-laden CCOFs, suggesting that multiple iodine species were captured by the CCOFs. The strong peaks at 167 cm^{-1} for all three iodine-laden CCOFs were attributed to the configuration of the coordinated pentaiodides I_5^-.[19,24,40] Meanwhile, the appearance of peaks at 143 cm^{-1} was attributed[23,40] to I_3^-. The appearance peaks at 110 and 134 cm^{-1} corresponded to both symmetric stretching vibration (ν_s) and asymmetric stretching (ν_{as}), respectively,[40] of I_3^- and I_5^-. The anion I_3^- and I_5^- species indicated that the charge transfer occurred between the guest iodine molecules and the electron-rich host network at CCOFs. Also, there are still small peaks at 180 and 194 cm^{-1}, which belong to the neutral iodine species.[40,41]

X-ray photoelectron spectroscopy (XPS) was further used to characterize the atomic structure of CCOFs, I_2-laden CCOFs, and iodine-binding species in CCOFs. The survey spectra (Figure 3d–f) showed new peaks near the binding energy of 619 eV for I_2-laden CCOFs, compared to the CCOFs ones, which were deconvoluted into the iodine components in the I_2-laden CCOFs. Then, high-resolution XPS spectra (Figure 3g–i) were conducted to identify the iodine-binding species in the I_2-laden CCOFs. For example, the raw data spectrum of COF-TpgTd (gray) was fitted with three components or chemical states (Figure 3i). The peaks at 619.84 eV (red) and 631.31 eV (blue) could be assigned to the neutral iodine $3d_{5/2}$ and $3d_{3/2}$ doublet signals, respectively. From the iodine database, we found that the $3d_{5/2}$ doublet peaks of cationic iodine species, like I_2O_5 and ICl_3, were located at the 623.30 and 622.50 eV, respectively. The $3d_{5/2}$ doublet peaks of anionic iodine species, such as KI and NaI, were close to 618.40–618.80 eV, respectively. Based on the above data, peaks at 622.28 eV (green) and 633.69 eV (purple) could be assigned to the $3d_{5/2}$ and $3d_{3/2}$ doublet peaks of the cationic iodine species, respectively, while peaks at 617.34 eV (yellow) and 628.28 (indigo) eV were attributed to the $3d_{5/2}$ and $3d_{3/2}$ doublet peaks of anionic iodine species, respectively. The other two CCOFs, COF-TpgBD and COF-TpgDB, exhibited very

https://dx.doi.org/10.1021/acsomega.0c02382
ACS Omega 2020, 5, 24262–24271

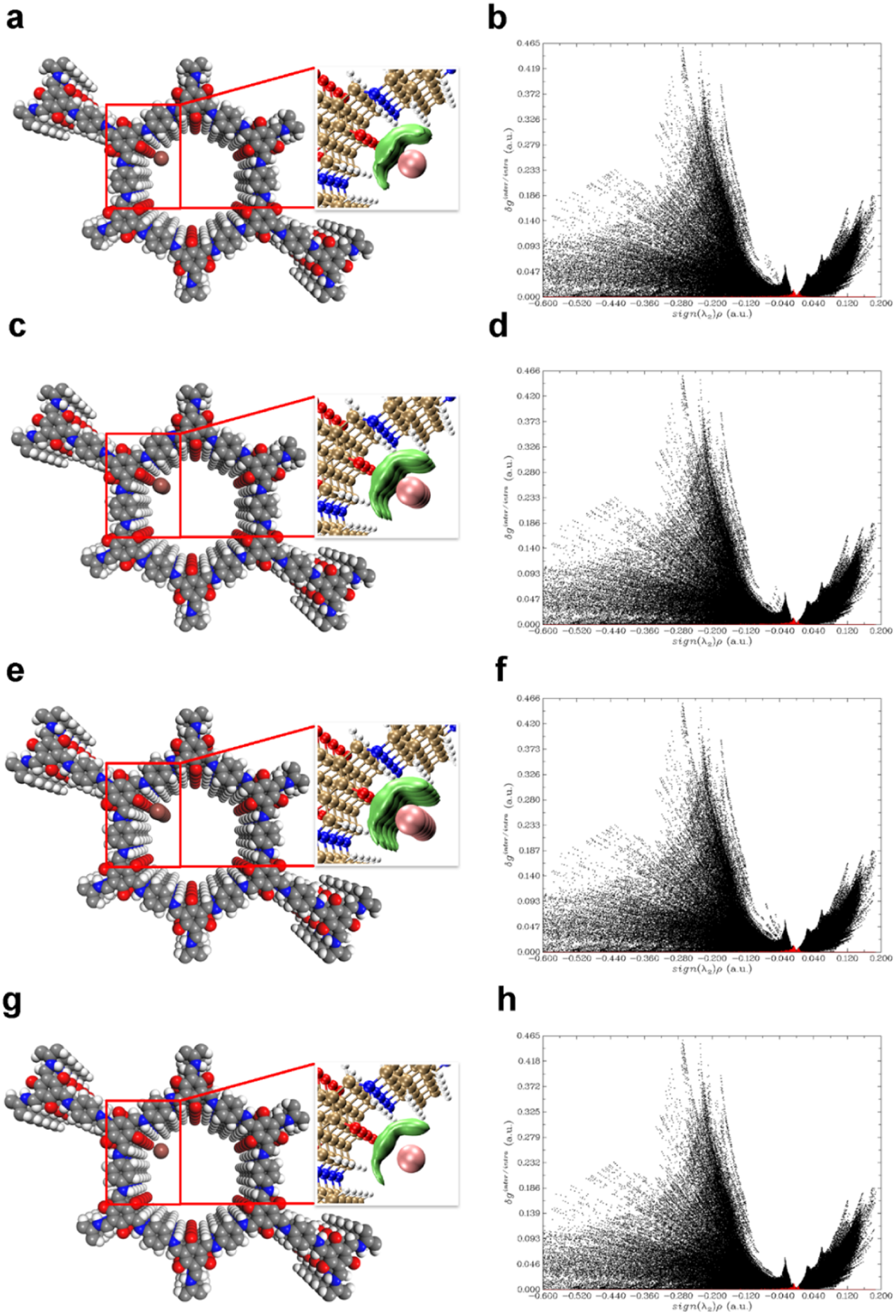

Figure 4. Simulated characterization of the iodine species capturing sites (Tpg) and IGM scatter plot of COF-TpgDB: (a, b) I_2; (c, d) I_3^-; (e, f) I_5^-; and (g, h) I^+.

similar iodine adsorption results as shown in Figure 3g,h. Obviously, four different iodine species with different valence states were strongly absorbed into the CCOFs.

To the best of our knowledge, no solid cationic iodine species have been reported in Raman spectroscopy. Therefore, it is hard to identify the cationic iodine species from the

https://dx.doi.org/10.1021/acsomega.0c02382
ACS Omega 2020, 5, 24262−24271

Raman patterns directly, although the XPS has pointed it loud and clear. Previous studies have showed that the cationic iodine species could be exited in the solution pyridines,[6] polyethylene matrix contained pyridines,[42] and hindered olefins adamantylideneadamantane[43] to form the so-called "homopolyatomic cations"[44,45] of nonmetallic elements. In Tpg residues of CCOFs, the −NH− and C═O functional groups constructed an electron-donor/acceptor network, which was analogous of Lewis acids and bases. Also, at the sterically hindered site, the iodine might be trapped and form cationic species.

As mentioned earlier, a good radioactive iodine adsorbent should have good capture ability of neutral and ionic iodine species. The above results offer strong evidence for the feasibility of CCOFs as powerful adsorbents.

2.2. Theoretical Calculation Analysis. DFT calculations were carried out to better understand the high adsorption efficacies of the CCOF iodine adsorbents. There are two possible adsorption sites inside the pores according to the topologies: one is located at the Tpg residues and the other at the diamine linker (DB, BD, and Td) residues. In Section 4, we confirm the presence of neutral (I_2), cationic (I^+), and anionic (I_3^- and I_5^-) species. To this end, all four iodine species at the two possible adsorption sites were investigated in this study. The calculations are illustrated in Figures 4 and S8−S12. Here, we took COF-TpgDB as an example to analyze the iodine species interacting with CCOFs. The first investigation was the neutral iodine I_2 absorbed at the Tpg residues sites of COF-TpgDB. At the Tpg adsorption site (Tpg···I_2), the shortest distances between I_2 and the ketone (C═O) and imine (>NH) functional groups were 3.43 (C═O···I_2) and 3.81 (> NH···I_2) angstrom (Å), respectively, which indicated that I_2 has been strongly attracted by the ketone and the imine functional groups (Figure 4a). An independent gradient model (IGM) descriptor (δg^{inter}) for the interaction between different fragments was further performed to identify and quantify the interactions between I_2 and CCOFs. The IGM descriptor δg plot as a function of sign(λ_2)ρ electronic density is shown in Figure 4b. Small sharp spikes were marked in red in the low-δg region, suggesting that the interaction between COF-TpgDB and I_2 was a hydrogen-bond interaction, with an average interaction of δg^{inter} = 0.08. The corresponding 3D isosurface (Figure 4a, inset) was also plotted to demonstrate the interaction between COF-TpgDB and I_2. Obviously, the neutral I_2 molecule is not only attracted by the COF-TpgDB layers it leans on but also strongly attracted by the up and down layers, thus creating a multiple-layer interaction network. At another diamine linker adsorption site (linker···I_2), the shortest distances between I_2 and the benzene hydrogen atom was 3.31 (Ph···I_2) Å, illustrating that I_2 also could be attracted by benzene functional groups (Figure S8a). The IGM results showed (Figure S8a inset and b) that the interaction of Ph···I_2 had an average δg^{inter} value of 0.04, which was weaker than that of Tpg···I_2.

The ionic state iodine molecules, I_3^-, I_5^-, and I^+, show very similar adsorption behaviors to that of I_2 in the COF-TpgDB pores. At the Tpg adsorption site (Tpg···I_3^-), the shortest distances between I_3^- and the ketone and imine were 3.41 (C═O···I_3^-) and 3.71 (>NH···I_3^-) Å, respectively, which were shorter compared with those of C═O···I_2 and 3.81 Å > NH···I_2 (Figure 4c). The IGM results also showed that the interaction δg^{inter} between I_3^- and COF-TpgDB had a larger average value of 0.11 and a much stronger hydrogen interaction (Figure 4d). At diamine linker adsorption site (linker···I_3^-), the shortest distances of Ph···I_3^- was 3.11 Å, and the average δg^{inter} value was 0.07 (Figure S8c,d), indicating that I_3^- was also significantly absorbed by the DB residues. Interestingly, I_5^- showed almost the same results (Figure 4e,f) with I_3^-. Similarly, the distances of C═O···I^+, >NH···I^+, and Ph···I^+ are 3.47, 3.78, and 3.14 Å (Figures 4g and S8g), respectively. The average δg^{inter} values of I^+ at the Tpg and DB adsorption sites are 0.09 and 0.07 (Figures 4h and S8h), respectively, indicating that COF-TpgDB also strongly absorbs I^+. Interestingly, I_3^-, I_5^-, and I^+ molecules interacted with multiple layers of COF-TpgDB to form an interaction network to enhance the iodine-capturing capability of COF-TpgDB.

The interaction between iodine and other two CCOFs, COF-TpgBD and COF-TpgTd, was the analogue of COF-TpgDB: multiple layers of CCOFs absorbed I_2, I_3^-, I_5^-, and I^+ molecules to generate an interaction network to maintain the iodine species (see the Supporting Information for more details). In addition, each layer of CCOFs had multiple adsorption sites, C═O, >NH, and Ph, to attract the iodine species, leading to significantly large adsorption energies (ΔG_{abs}; Table 1). For example, ΔG_{abs} of Ph···I^+ at COF-TpgDB linker sites had the lowest adsorption energy of 151.74 kcal/mol, but it was still higher than those of other porous materials such as ZIF-8[15] and MFP.[17] Our adsorbent materials have more adsorption sites and higher adsorption energies than ZIF-8 which case CCOFs have higher iodine-loading ratios than ZIF-8. The interaction network of I_2, I_3^-, I_5^-, and I^+ molecules and multiple layers of CCOFs was similar to the MFP-I_3^- network reported by Wang et al.[17] Although the surface areas of CCOFs were not as high as the iodine-loading ratios of MFP, the high adsorption energies make iodine hard to be completely removed from CCOFs after multiple washing cycles with different solutions, suggesting the potential of CCOFs in stabilizing the absorbed radiational iodine.

Table 1. Adsorption Energy (ΔG_{abs}) of CCOFs[a]

compound	ΔG_{abs}, I_2	ΔG_{abs}, I_3^-	ΔG_{abs}, I_5^-	ΔG_{abs}, I^+
COF-TpgDB Tpg sites	198.08	195.66	236.74	151.93
COF-TpgDB DB sites	198.88	195.43	316.59	151.74
COF-TpgBD Tpg sites	283.60	300.54	390.70	235.28
COF-TpgBD BD sites	284.67	281.91	408.77	195.66
COF-TpgTd Tpg sites	204.72	217.68	252.51	247.98
COF-TpgTd Td sites	205.99	209.32	334.91	236.84

[a]Unit for ΔG_{abs} is kcal/mol.

3. CONCLUSIONS

In summary, we have successfully synthesized a series of CCOF materials suitable for capturing and maintaining not only neutral I_2 molecules but ionic state (I_3^-, I_5^-, and I^+) iodine species for the first time. In this study, we have proposed an innovative method for convenient and large-scale production of CCOFs under ambient conditions. The CCOFs achieved 260, 181, and 166 wt % adsorption capacity toward iodine, respectively. Moreover, the captured iodine is hard to remove from CCOF materials by various treatments, rendering them suitable for long-term adsorption and radiational iodine sequestration. More importantly, we conducted a detailed experimental investigation to analyze the adsorption of iodine species in CCOFs, revealing that neutral and ionic iodine species are both efficiently captured by CCOFs. Finally,

https://dx.doi.org/10.1021/acsomega.0c02382
ACS Omega 2020, 5, 24262−24271

Scheme 1. Construction of COF-TpgDB, COF-TpgBD, and COF-TpgTd

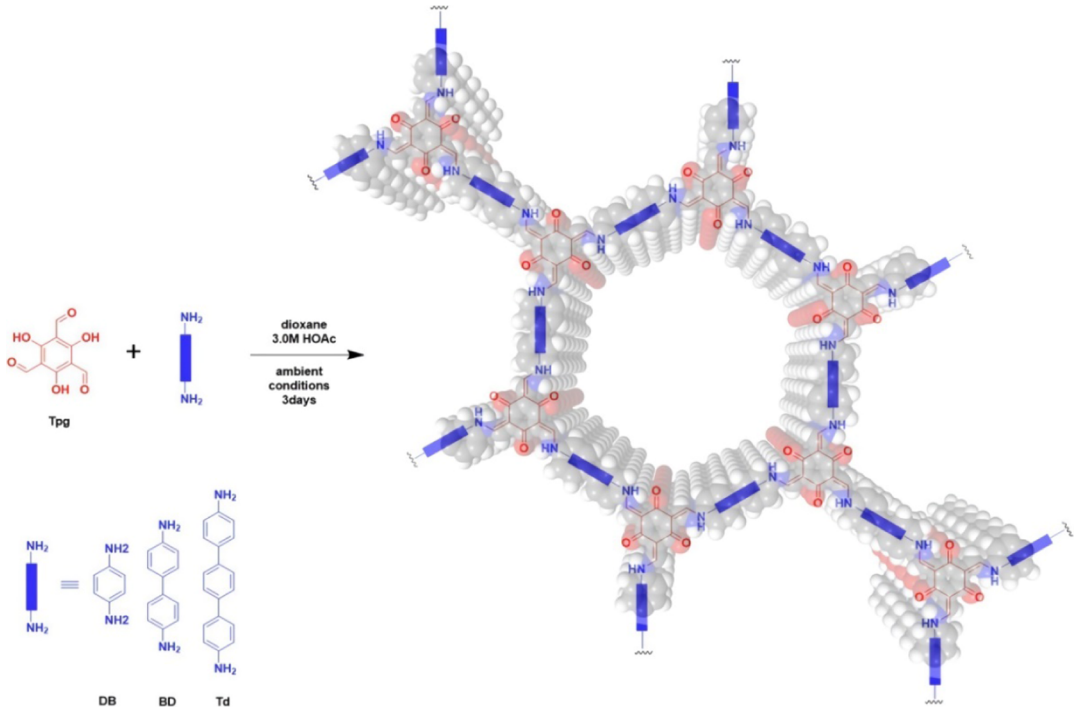

theoretical calculations were employed to study the adsorption sites in the CCOFs for different iodine species, clearly demonstrating the relationship between different functional groups and different iodine species and providing the basis for the design and development of more advanced adsorbent materials.

4. EXPERIMENTAL SECTION

4.1. Materials. 2,4,6-Trihydroxylbenzene-1,3,5-tricarbaldehyde (Tpg), 1,4-diaminebenzene (DB), benzidine (BD), and 4,4″-diamino-*p*-terphenyl (Td) were purchased from Jilin Chinese Academy of Science, Yanshen Technology Co., Ltd. 1,4-Dioxane,*N*,*N*-dimethylformamide (DMF), acetone, and tetrahydrofuran (THF) were purchased from Beijing Chemical Industry Co., Ltd. All chemical reagents were analytical grade and used as received without further purification.

4.2. Synthesis of Covalent Organic Frameworks (COFs). The previous synthesis of CCOFs[37,39] was carried out under the flame-seal and high-temperature conditions. Here, we proposed an improved method of facilitate the large-scale production CCOFs at room temperature without harsh synthesis conditions, as shown in Scheme 1. Typically, 2,4,6-trihydroxybenzene-1,3,5-tricarbaldehyde (Tpg, 0.3 mmol, 63 mg) and diamine linker (DB, BD, and Td, 0.45 mmol) were added into a vial and suspended in 3 mL of 1,4-dioxane. Aqueous acetic acid (0.6 mL, 3 M) was added to the mixture at room temperature. The suspensions were placed in a refrigerator at 7 °C for 3 days. The precipitate was then isolated by centrifugation and washed with *N*,*N*-dimethylformamide (6 × 4 mL) and acetone (6 × 4 mL) sequentially. Further purification was carried out by Soxhlet extraction in tetrahydrofuran for 24 h and acetone for 24 h and dried at 80 °C under vacuum for 72 h to obtain dried CCOF powder. Compared to other iodine adsorbents, the C−N-linked COFs were much easier for industrial synthesis and lower cost. In the case of extreme circumstances, for example, the nuclear radiation leakage in Fukushima plant, faster and larger facilitated synthesis of adsorbents is the key to contain the leakage.

4.3. Adsorption Experiment. *4.3.1. Iodine Adsorption Measurements.* A small vessel containing 100 mg of COF powder was placed in a hermetically sealed desiccator with solid iodine in the bottom. The iodine adsorption experiment was performed at 75 °C and ambient pressure under static conditions. The cooled vessel was weighed at various intervals (0−72 h). The iodine adsorption capacity was calculated by eq 1 as follows

$$q = \frac{(m_t - m_0)}{m_0} \quad (1)$$

where q (g/g) is the amount of iodine adsorbed by per gram of adsorbent at time t (min). m_t (g) and m_0 are the amounts of adsorbent at the initial and time, t, respectively. All experimental results were performed with triple parallel experiments.

4.4. Characterization. The FT-IR (KBr pellet) spectra were recorded in the wavenumber range of 4000−400 cm^{-1} using a Nicolet 360 FT-IR spectrophotometer. Nitrogen sorption was measured with a Quadrachorme adsorption instrument at 77.3 K after degassing the sample for 8 h under vacuum at 120 °C. The Brunauer−Emmett−Teller (BET) surface areas were calculated from the adsorption branch. Powder X-ray diffraction (PXRD) measurements were carried out in reflection mode on a D/max-2550 type X-ray diffractometer with Cu Kα radiation (λ = 1.54060 Å) at a working voltage of 40 kV and a current of 40 mA. The scanning rate is 1° min^{-1}, and the scanning range is 2−35°. Scanning electron microscopy (SEM) was performed on a XL-30 field emission scanning electron microscope at acceleration voltages of 1 kV. The sample was dispersed ultrasonically in ethanol and dropped onto a silicon wafer. Transmission electron microscopy (TEM) images were obtained with a

https://dx.doi.org/10.1021/acsomega.0c02382
ACS Omega 2020, 5, 24262−24271

TECNAI G2 high-resolution transmission electron microscope at an acceleration voltage of 200 kV. The XPS spectra were obtained by a VG ESCALAB MKII X-ray photoelectron spectrometer. Thermogravimetric analysis (TGA) was conducted using a PerkinElmer TGA-2 thermogravimetric analyzer in N_2 from room temperature to 1000 °C at a rate of 10 °C min^{-1}. The solid-state ^{13}C NMR measurements were conducted using AVANCE III 400 WB solid 400 MHz (wide cavity) superconducting nuclear magnetic resonance spectrometer. The Raman spectrum was obtained using a Renishaw InVia Reflex equipped with a 785 nm diode laser.

5. COMPUTATIONAL SECTION

The electronic structures of CCOFs were evaluated with CP2K Quickstep[46,47] module at xTB[48] level. Van der Waals interaction was described using the D3[49,50] method. The unit cells of all CCOFs were fully optimized with no constrain. Supercells (2 × 2 × 6) were used to investigate the interaction between the iodine species and the CCOFs. The weak attractive interactions between all of the three of iodine species and the CCOFs were studied by independent gradient model (IGM) analysis, which is described by Lefebvre and his coworkers.[51] The IGM interactions were calculated with Multiwfn[52,53] software, and the gradient isosurface were plotted with VMD[54] software.

The adsorption energy (ΔG_{abs}) was calculated by the following formula

$$\Delta G_{abs} = \Delta G_{COF-iodine} - \Delta G_{COF} - \Delta G_{iodine} \quad (2)$$

where $\Delta G_{COF\text{-}iodine}$, ΔG_{COF}, and ΔG_{iodine} are the Gibbs free energies of the iodine-laden CCOFs, pristine CCOFs, and iodine, respectively.

■ ASSOCIATED CONTENT

Supporting Information

The Supporting Information is available free of charge at https://pubs.acs.org/doi/10.1021/acsomega.0c02382.

PXRD patterns of CCOFs including chemical structural formula, N_2 adsorption and desorption isotherms of CCOFs, thermogravimetric analysis, TEM images, theoretical calculations and analysis and tables (PDF)

■ AUTHOR INFORMATION

Corresponding Authors

Linfeng Gan − *Changchun Institute of Applied Chemistry, Chinese Academy of Sciences, Changchun, Jilin 130022, China*; orcid.org/0000-0002-9589-5817; Email: lfgan@qq.com

Yuanrui Wang − *School of Chemical Engineering, Changchun University of Technology, Changchun, Jilin 130012, China*; Email: wyr@ccut.edu.cn

Authors

Yonghe Sun − *School of Chemical Engineering, Changchun University of Technology, Changchun, Jilin 130012, China*

Sanan Song − *College of Chemistry, Jilin University, Changchun, Jilin 130012, China*

Dehai Xiao − *Changchun Institute of Applied Chemistry, Chinese Academy of Sciences, Changchun, Jilin 130022, China*

Complete contact information is available at: https://pubs.acs.org/10.1021/acsomega.0c02382

Notes

The authors declare no competing financial interest.

■ ACKNOWLEDGMENTS

We gratefully acknowledge the financial support received from the Science and Technology Department of Jilin Province (No. 20190201234JC) and Computing Centre of Jilin Province.

■ REFERENCES

(1) Vienna, J. D. Nuclear Waste Vitrification in the United States: Recent Developments and Future Options. *Int. J. Appl. Glass Sci.* **2010**, *1*, 309−321.

(2) Kintisch, E. Nuclear power - Congress tells DOE to take fresh look at recycling spent reactor fuel. *Science* **2005**, *310*, No. 1406.

(3) Ojovan, M.; Lee, W. *An Introduction to Nuclear Waste Immobilisation*; Elsevier Science, 2005.

(4) Demartin, F.; Deplano, P.; Devillanova, F. A.; Isaia, F.; Lippolis, V.; Verani, G. Conductivity, Ft-Raman Spectra, and X-Ray Crystal-Structures of 2 Novel [D2i]in (N = 3 and D = N-Methylbenzothiazole-2(3h)-Selone - N = 7 and D = N-Methylbenzothiazole-2(3h)-Thione) Iodonium Salts - 1st Example of I-.3i2 Heptaiodide. *Inorg. Chem.* **1993**, *32*, 3694−3699.

(5) Diel, B. N.; Inabe, T.; Lyding, J. W.; Schoch, K. F.; Kannewurf, C. R.; Marks, T. J. Cofacial Assembly of Partially Oxidized Metallomacrocycles as an Approach to Controlling Lattice Architecture in Low-Dimensional Molecular-Solids - Chemical, Structural, Oxidation-State, Transport, Magnetic, and Optical-Properties of Halogen-Doped [M(Phthalocyaninato)O]N Macromolecules, Where M = Si, Ge, and Sn. *J. Am. Chem. Soc.* **1983**, *105*, 1551−1567.

(6) Hassel, O.; Hope, H. Structure of Solid Compound Formed by Additionof. 2. Molecules of Iodine To. 1. Molecule of Pyridine. *Acta Chem. Scand.* **1961**, *15*, 407−416.

(7) Herbstein, F. H.; Schwotzer, W. Polyiodide Salts and Molecular-Complexes. 7. Interaction of Thiones with Molecular Diiodine - the Crystal-Structures of Dithizone Diiodine, Ethylenethiourea-Bis-(Diiodine), Bis(Ethylenethiourea)-Tris(Diiodine), Bis(Dithizone)-Heptakis(Diiodine), and 1-(1-Imidazolin-2-Yl)-2-Thioxoimidazolidinium Triiodide-(Ethylenethiourea-Diiodine). *J. Am. Chem. Soc.* **1984**, *106*, 2367−2373.

(8) Riley, B. J.; Vienna, J. D.; Strachan, D. M.; McCloy, J. S.; Jerden, J. L. Materials and processes for the effective capture and immobilization of radioiodine: A review. *J. Nucl. Mater.* **2016**, *470*, 307−326.

(9) Nandanwar, S. U.; Coldsnow, K.; Utgikar, V.; Sabharwall, P.; Aston, D. E. Capture of harmful radioactive contaminants from off-gas stream using porous solid sorbents for clean environment - A review. *Chem. Eng. J.* **2016**, *306*, 369−381.

(10) Chapman, K. W.; Chupas, P. J.; Nenoff, T. M. Radioactive iodine capture in silver-containing mordenites through nanoscale silver iodide formation. *J. Am. Chem. Soc.* **2010**, *132*, 8897−8899.

(11) Subrahmanyam, K. S.; Sarma, D.; Malliakas, C. D.; Polychronopoulou, K.; Riley, B. J.; Pierce, D. A.; Chun, J.; Kanatzidis, M. G. Chalcogenide Aerogels as Sorbents for Radioactive Iodine. *Chem. Mater.* **2015**, *27*, 2619−2626.

(12) Riley, B. J.; Chun, J.; Um, W.; Lepry, W. C.; Matyas, J.; Olszta, M. J.; Li, X.; Polychronopoulou, K.; Kanatzidis, M. G. Chalcogen-Based Aerogels As Sorbents for Radionuclide Remediation. *Environ. Sci. Technol.* **2013**, *47*, 7540−7547.

(13) Chapman, K. W.; Sava, D. F.; Halder, G. J.; Chupas, P. J.; Nenoff, T. M. Trapping Guests within a Nanoporous Metal−Organic Framework through Pressure-Induced Amorphization. *J. Am. Chem. Soc.* **2011**, *133*, 18583−18585.

(14) Sava, D. F.; Rodriguez, M. A.; Chapman, K. W.; Chupas, P. J.; Greathouse, J. A.; Crozier, P. S.; Nenoff, T. M. Capture of volatile iodine, a gaseous fission product, by zeolitic imidazolate framework-8. *J. Am. Chem. Soc.* **2011**, *133*, 12398−12401.

(15) Hughes, J. T.; Sava, D. F.; Nenoff, T. M.; Navrotsky, A. Thermochemical Evidence for Strong Iodine Chemisorption by ZIF-8. *J. Am. Chem. Soc.* **2013**, *135*, 16256−16259.
(16) Sava, D. F.; Garino, T. J.; Nenoff, T. M. Iodine Confinement into Metal−Organic Frameworks (MOFs): Low-Temperature Sintering Glasses To Form Novel Glass Composite Material (GCM) Alternative Waste Forms. *Ind. Eng. Chem. Res.* **2012**, *51*, 614−620.
(17) Wang, J.; Li, Z. L.; Wang, Y.; Wei, C. T.; Ai, K. L.; Lu, L. H. Hydrogen bond-mediated strong adsorbent-I_3^- interactions enable high-efficiency radioiodine capture. *Mater. Horiz.* **2019**, *6*, 1517−1525.
(18) Yan, Z.; Yuan, Y.; Tian, Y.; Zhang, D.; Zhu, G. Highly Efficient Enrichment of Volatile Iodine by Charged Porous Aromatic Frameworks with Three Sorption Sites. *Angew. Chem.* **2015**, *127*, 12924−12928.
(19) Pei, C.; Ben, T.; Xu, S.; Qiu, S. Ultrahigh iodine adsorption in porous organic frameworks. *J. Mater. Chem. A* **2014**, *2*, 7179−7187.
(20) Li, Y. Q.; Li, Y. R.; Zhao, Q. H.; Li, L.; Chen, R.; He, C. Y. Cotton fiber functionalized with 2D covalent organic frameworks for iodine capture. *Cellulose* **2020**, *27*, 1517−1529.
(21) Pan, X. W.; Qin, X. H.; Zhang, Q. H.; Ge, Y. S.; Ke, H. Z.; Cheng, G. E. N- and S-rich covalent organic framework for highly efficient removal of indigo carmine and reversible iodine capture. *Microporous Mesoporous Mater.* **2020**, *296*, No. 109990.
(22) Huang, M.; Yang, L.; Li, X. Y.; Chang, G. J. An indole-derived porous organic polymer for the efficient visual colorimetric capture of iodine in aqueous media via the synergistic effects of cation-pi and electrostatic forces. *Chem. Commun.* **2020**, *56*, 1401−1404.
(23) Li, J.; Zhang, H.; Zhang, L.; Wang, K.; Wang, Z.; Liu, G.; Zhao, Y.; Zeng, Y. Two-dimensional covalent−organic frameworks for ultrahigh iodine capture. *J. Mater. Chem. A* **2020**, *8*, 9523−9527.
(24) Xu, M. Y.; Wang, T.; Zhou, L.; Hua, D. B. Fluorescent conjugated mesoporous polymers with N,N-diethylpropylamine for the efficient capture and real-time detection of volatile iodine. *J. Mater. Chem. A* **2020**, *8*, 1966−1974.
(25) Geng, T. M.; Zhang, C.; Liu, M.; Hu, C.; Chen, G. F. Preparation of biimidazole-based porous organic polymers for ultrahigh iodine capture and formation of liquid complexes with iodide/polyiodide ions. *J. Mater. Chem. A* **2020**, *8*, 2820−2826.
(26) Janeta, M.; Bury, W.; Szafert, S. Porous Silsesquioxane Imine Frameworks as Highly Efficient Adsorbents for Cooperative Iodine Capture. *ACS Appl. Mater. Interfaces* **2018**, *10*, 19964−19973.
(27) Côté, A. P.; Benin, A. I.; Ockwig, N. W.; O'Keeffe, M.; Matzger, A. J.; Yaghi, O. M. Porous, crystalline, covalent organic frameworks. *Science* **2005**, *310*, 1166−1170.
(28) Wang, H.; Zeng, Z. T.; Xu, P.; Li, L. S.; Zeng, G. M.; Xiao, R.; Tang, Z. Y.; Huang, D. L.; Tang, L.; Lai, C.; Jiang, D. N.; Liu, Y.; Yi, H.; Qin, L.; Ye, S. J.; Ren, X. Y.; Tang, W. W. Recent progress in covalent organic framework thin films: fabrications, applications and perspectives. *Chem. Soc. Rev.* **2019**, *48*, 488−516.
(29) Geng, K.; He, T.; Liu, R.; Dalapati, S.; Tan, K. T.; Li, Z.; Tao, S.; Gong, Y.; Jiang, Q.; Jiang, D. Covalent Organic Frameworks: Design, Synthesis, and Functions. *Chem. Rev.* **2020**, *120*, 8814−8933.
(30) Zhang, S. N.; Zheng, Y. L.; An, H. D.; Aguila, B.; Yang, C. X.; Dong, Y. Y.; Xie, W.; Cheng, P.; Zhang, Z. J.; Chen, Y.; Ma, S. Q. Covalent Organic Frameworks with Chirality Enriched by Biomolecules for Efficient Chiral Separation. *Angew. Chem., Int. Ed.* **2018**, *57*, 16754−16759.
(31) Guan, X.; Li, H.; Ma, Y.; Xue, M.; Fang, Q.; Yan, Y.; Valtchev, V.; Qiu, S. Chemically stable polyarylether-based covalent organic frameworks. *Nat. Chem.* **2019**, *11*, 587−594.
(32) Yan, S. C.; Guan, X. Y.; Li, H.; Li, D. H.; Xue, M.; Yan, Y. S.; Valtchev, V.; Qiu, S. L.; Fang, Q. R. Three-dimensional Salphen-based Covalent Organic Frameworks as Catalytic Antioxidants. *J. Am. Chem. Soc.* **2019**, *141*, 2920−2924.
(33) Ongari, D.; Yakutovich, A. V.; Talirz, L.; Smit, B. Building a Consistent and Reproducible Database for Adsorption Evaluation in Covalent−Organic Frameworks. *ACS Cent. Sci.* **2019**, *5*, 1663−1675.
(34) Wang, C.; Wang, Y.; Ge, R. L.; Song, X. D.; Xing, X. Q.; Jiang, Q. K.; Lu, H.; Hao, C.; Guo, X. W.; Gao, Y. A.; Jiang, D. L. A 3D Covalent Organic Framework with Exceptionally High Iodine Capture Capability. *Chem. - Eur. J.* **2018**, *24*, 585−589.
(35) Yin, Z. J.; Xu, S. Q.; Zhan, T. G.; Qi, Q. Y.; Wu, Z. Q.; Zhao, X. Ultrahigh volatile iodine uptake by hollow microspheres formed from a heteropore covalent organic framework. *Chem. Commun.* **2017**, *53*, 7266−7269.
(36) Wang, P.; Xu, Q.; Li, Z. P.; Jiang, W. M.; Jiang, Q. H.; Jiang, D. L. Exceptional Iodine Capture in 2D Covalent Organic Frameworks. *Adv. Mater.* **2018**, *30*, No. 1801991.
(37) Kandambeth, S.; Mallick, A.; Lukose, B.; Mane, M. V.; Heine, T.; Banerjee, R. Construction of crystalline 2D covalent organic frameworks with remarkable chemical (acid/base) stability via a combined reversible and irreversible route. *J. Am. Chem. Soc.* **2012**, *134*, 19524−19527.
(38) Ding, S. Y.; Gao, J.; Wang, Q.; Zhang, Y.; Song, W. G.; Su, C. Y.; Wang, W. Construction of covalent organic framework for catalysis: Pd/COF-LZU1 in Suzuki-Miyaura coupling reaction. *J. Am. Chem. Soc.* **2011**, *133*, 19816−19822.
(39) Han, X.; Zhang, J.; Huang, J.; Wu, X.; Yuan, D.; Liu, Y.; Cui, Y. Chiral induction in covalent organic frameworks. *Nat. Commun.* **2018**, *9*, No. 1294.
(40) Svensson, P. H.; Kloo, L. Synthesis, structure, and bonding in polyiodide and metal iodide-iodine systems. *Chem. Rev.* **2003**, *103*, 1649−1684.
(41) Svensson, P. H.; Gorlov, M.; Kloo, L. Dimensional Caging of Polyiodides. *Inorg. Chem.* **2008**, *47*, 11464−11466.
(42) Nguyen, H. T.; Nguyen, D. D.; Spanget-Larsen, J. Ionic reaction products of iodine with pyridine, 4-methylpyridine, and 4-tert-butylpyridine in a polyethylene matrix. A FTIR polarization spectroscopic investigation. *Chem. Phys. Lett.* **2019**, *716*, 119−125.
(43) Brown, R. S.; Nagorski, R. W.; Bennet, A. J.; Mcclung, R. E. D.; Aarts, G. H. M.; Klobukowski, M.; Mcdonald, R.; Santarsiero, B. D. Stable Bromonium and Iodonium Ions of the Hindered Olefins Adamantylideneadamantane and Bicyclo[3.3.1]-Nonylidenebicyclo[3.3.1]Nonane - X-Ray Structure, Transfer of Positive Halogens to Acceptor Olefins, and Ab-Initio Studies. *J. Am. Chem. Soc.* **1994**, *116*, 2448−2456.
(44) Engesser, T. A.; Krossing, I. Recent advances in the syntheses of homopolyatomic cations of the non metallic elements C, N, P, S, Cl, Br, I and Xe. *Coord. Chem. Rev.* **2013**, *257*, 946−955.
(45) Engesser, T. A.; Lichtenthaler, M. R.; Schleep, M.; Krossing, I. Reactive p-block cations stabilized by weakly coordinating anions. *Chem. Soc. Rev.* **2016**, *45*, 789−899.
(46) Hutter, J.; Iannuzzi, M.; Schiffmann, F.; VandeVondele, J. CP2K: atomistic simulations of condensed matter systems. *WIREs Comput. Mol. Sci.* **2014**, *4*, 15−25.
(47) VandeVondele, J.; Krack, M.; Mohamed, F.; Parrinello, M.; Chassaing, T.; Hutter, J. QUICKSTEP: Fast and accurate density functional calculations using a mixed Gaussian and plane waves approach. *Comput. Phys. Commun.* **2005**, *167*, 103−128.
(48) Grimme, S.; Bannwarth, C.; Shushkov, P. A Robust and Accurate Tight-Binding Quantum Chemical Method for Structures, Vibrational Frequencies, and Noncovalent Interactions of Large Molecular Systems Parametrized for All spd-Block Elements (Z = 1-86). *J. Chem. Theory. Comput.* **2017**, *13*, 1989−2009.
(49) Grimme, S.; Ehrlich, S.; Goerigk, L. Effect of the damping function in dispersion corrected density functional theory. *J. Comput. Chem.* **2011**, *32*, 1456−1465.
(50) Grimme, S.; Antony, J.; Ehrlich, S.; Krieg, H. A consistent and accurate ab initio parametrization of density functional dispersion correction (DFT-D) for the 94 elements H-Pu. *J. Chem. Phys.* **2010**, *132*, No. 154104.
(51) Lefebvre, C.; Rubez, G.; Khartabil, H.; Boisson, J. C.; Contreras-Garcia, J.; Henon, E. Accurately extracting the signature of intermolecular interactions present in the NCI plot of the reduced density gradient versus electron density. *Phys. Chem. Chem. Phys.* **2017**, *19*, 17928−17936.

https://dx.doi.org/10.1021/acsomega.0c02382
ACS Omega 2020, 5, 24262−24271

(52) Johnson, E. R.; Keinan, S.; Mori-Sanchez, P.; Contreras-Garcia, J.; Cohen, A. J.; Yang, W. T. Revealing Noncovalent Interactions. *J. Am. Chem. Soc.* **2010**, *132*, 6498−6506.
(53) Lu, T.; Chen, F. W. Multiwfn: A multifunctional wavefunction analyzer. *J. Comput. Chem.* **2012**, *33*, 580−592.
(54) Humphrey, W.; Dalke, A.; Schulten, K. VMD: Visual molecular dynamics. *J. Mol. Graphics* **1996**, *14*, 33−38.

https://dx.doi.org/10.1021/acsomega.0c02382
ACS Omega 2020, 5, 24262−24271